Clay Minerals (2023), **58**, 415–423
doi:10.1180/clm.2023.38

CAMBRIDGE UNIVERSITY PRESS

Article

Molecular dynamics simulation of dodecyl dimethyl benzyl ammonium cation-intercalated montmorillonite

Haotian Su[1], Yingchun Zhang[1], Jinhong Zhou[1]* and Qingfeng Hou[2]

[1]State Key Laboratory for Mineral Deposits Research, School of Earth Sciences and Engineering, Nanjing University, Nanjing, Jiangsu, P.R. China and [2]State Key Laboratory of Enhanced Oil Recovery, Research Institute of Petroleum Exploration and Development, China National Petroleum Corporation (CNPC), Beijing, P.R. China

Abstract

Dodecyl dimethyl benzyl ammonium (DDBA) is a novel cation surfactant used to modify clay minerals. DDBA-intercalated montmorillonite is formed by the ion exchange between DDBA cations in the solution and cations in the montmorillonite interlayers. By using molecular dynamics simulations, we investigated the basal spacings, interlayer structures and dynamics of DDBA-montmorillonites. The results showed that the calculated basal spacings agreed well with experimental values and that the layering behaviours of DDBA had been revealed. The ammonium groups of DDBA ions preferred staying close to the centre of Si–O six-member rings. The benzyl group and lauryl group were oriented in parallel in the monolayer state, whereas they were tilted in other states. DDBA ions have very low mobility in the interlayer region, indicating that the negatively charged montmorillonite surfaces can effectively fix this positively charged surfactant. The microscopic structures and dynamics obtained in the present study provide atomic-scale insights into the properties of DDBA-intercalated clay minerals.

Keywords: Dodecyl dimethyl benzyl ammonium; interlayer structure; mobility; molecular dynamics simulation; montmorillonite

(Received 9 October 2023; revised 23 December 2023; accepted 25 December 2023; Associate Editor: Chunhui Zhou)

Montmorillonite (Mnt) is the most common 2:1 clay mineral. The negative layer charge of Mnt originates from the isomorphic substitution, including octahedral substitution (Mg for Al) and tetrahedral substitution (Al for Si; Brigatti *et al.*, 2006). Exchangeable hydrated metal cations exist in the interlayer of Mnt. Organoclays can be formed through ion exchange between these metal cations and organic cations. Organoclays have been proven to be versatile materials in industry, with a wide range of applications as adsorbents, rheological control agents and components of oil well drilling fluids (Yariv & Cross, 2002; Lagaly *et al.*, 2006; Park *et al.*, 2011; Bhatt *et al.*, 2013; Silva *et al.*, 2014; Shah *et al.*, 2018).

In the synthesis of organoclays, alkylammonium cations are favoured surface modifiers due to their affordability and ease of preparation (Gieseking, 1939; Nigam *et al.*, 2004). Many experiments have been conducted to investigate the properties of alkylammonium-intercalated Mnt (Barrer & MacLeod, 1995; Bala *et al.*, 2000; Scholtzová *et al.*, 2016; Veiskarami *et al.*, 2016; Peng *et al.*, 2018). Tetraalkylammonium-modified Mnt exhibits remarkable adsorption capacity for benzene, with tetramethylammonium being particularly effective (Chun *et al.*, 2003). In other studies, Mnt modified with dodecyl trimethylammonium or dioctadecyl dimethylammonium cations has been utilized for the adsorption and degradation of chlorobenzene (Witthuhn *et al.*, 2006).

In recent years, the dodecyl dimethyl benzyl ammonium (DDBA) ion has been analysed by increasing numbers of researchers (Khan *et al.*, 2017; Fellah *et al.*, 2021; Ilari *et al.*, 2021; Barber & Hartmann, 2022; Zeng *et al.*, 2022). As a quaternary ammonium organic cation, DDBA is composed of a positively charged N atom linked with a lauryl group (12-C alkyl chain), a benzyl group and two methyl groups (Van de Voorde *et al.*, 2012; Zanini *et al.*, 2013). DDBA, as one of *n*-alkyl dimethyl benzyl ammonium cationic surfactants, is used to prepare organoclays (n = the number of carbon atoms in the alkyl chain). Kwolek *et al.* (2003) experimentally determined the adsorption capacities and structures of homologues (*n*-alkyl dimethyl benzyl ammonium, n = 2, 4, …, 10, 12) with different alkyl chain carbon numbers, including DDBA, in Mnt interlayers. Tahani *et al.* (1999) measured the different basal spacings and interlayer structures of DDBA-intercalated Mnt with various loadings. Fellah *et al.* (2021) experimentally compared the adsorption capacities of DDBA and sodium dodecyl sulfate surfactants on kaolinite surfaces. Moreover, DDBA has the characteristics of both a cationic surfactant and a disinfectant (the main component of benzalkonium; Flores *et al.*, 2017); therefore, it was used as an environmental bactericidal and antifungal agent. DDBA-Mnt can be used as a carrier to exert a sustained antibacterial or anti-mildew effect in the environment (Yue *et al.*, 2019). Yue *et al.* (2019) measured the basal spacing of DDBA-Mnt and the release rate of DDBA-Mnt in water. Zanini *et al.* (2013) compared the differences in adsorption between DDBA and other benzalkonium

*Corresponding author: Jinhong Zhou; Email: zjh12387@126.com
Cite this article: Su H, Zhang Y, Zhou J, Hou Q (2023). Molecular dynamics simulation of dodecyl dimethyl benzyl ammonium cation-intercalated montmorillonite. *Clay Minerals* **58**, 415–423. https://doi.org/10.1180/clm.2023.38

main components (tetradecyl dimethyl benzyl ammonium) in Mnt interlayers. In other applications, DDBA-modified rectorite has been successfully utilized for the adsorption of phenol from solution and used as a filler additive to modify gel polymer electrolytes (Huang *et al.*, 2007, 2008, 2009, 2010). The use of DDBA-modified Mnt to adsorb the antibiotics ampicillin and amoxicillin has also been studied (Li *et al.*, 2021). The intercalation of DDBA in Mnt was used as a structure-directing agent in the synthesis of Fe-incorporated silica-pillared clays, which can be used for catalysis, adsorption and separation (Yang *et al.*, 2012, 2013). However, although DDBA-modified clays (i.e. DDBA-intercalated clays) have been widely studied and applied, the most common model of the DDBA arrangement between clay layers requires more detail. The microscopic structure and dynamics of DDBA in the interlayer of Mnt have not been clearly revealed.

Molecular simulation has proven to be a powerful tool for elucidating the microscopic structures and dynamics of organoclay systems, providing complementary results to experimental findings (Cygan *et al.*, 2012, 2021; Teich-McGoldrick *et al.*, 2015; Scholtzová, 2020). Minisini & Tsobnang (2005) used the COMPASS force field (Sun, 1998) to simulate an alkylammonium surfactant with only one alkyl chain-intercalated Mnt system. Their simulation results accurately reproduced the X-ray diffraction (XRD) measurements of basal spacings reported by Hackett *et al.* (1998). Heinz *et al.* (2006) employed the PCFF force field (Sun *et al.*, 1994) to determine the cleavage energy at the interface of octadecyl ammonium and Mnt. The calculated cleavage energies and their Coulomb and van der Waals contributions were found to be in good agreement with experimental results (Giese & Van Oss, 2002; Yariv & Cross, 2002). Lanson *et al.* (2022) simulated the behaviour of alkylammonium in the Mnt interlayer using Amber–ClayFF force fields (Cornell *et al.*, 1995; Pearlman *et al.*, 1995; Cygan *et al.*, 2004) and obtained stable configurations; the calculated basal spacing were close to experimental values (Lagaly & Weiss, 1971; Lagaly, 1994). Liu *et al.* (2007) investigated the swelling behaviour of alkylammonium-intercalated smectites as a function of carbon chain length by using the combined ClayFF–CVFF force field (Dauber-Osguthorpe *et al.*, 1988; Cygan *et al.*, 2004). The simulation results of the system basal spacings agree with the experimental findings of alkylammonium-intercalated smectites as reported by Laird *et al.* (1989). Zhou *et al.* (2014) utilized the same combined force field to derive the structural and dynamic properties of water-saturated cetyltrimethylammonium-Mnt. Their simulation findings were consistent with experimental basal spacing and the conformation of alkyl chains (Kung & Hayes, 1993; Zhu *et al.*, 2008). Ghavami *et al.* (2017) determined the alterations in basal spacing of hexadecyltrimethylammonium-Mnt by adsorption of organic solvents such as naphthalene. They used the ClayFF–CVFF force field in combination with XRD, transmission electron microscopy (TEM) and Fourier-transform infrared (FTIR) spectrometry experimental methods to establish that the simulation outcomes closely matched the experimental results. These studies verified that the ClayFF–CVFF force field can accurately reproduce the microscopic properties of organic-intercalated clay minerals.

In this study, we focused on the interaction between DDBA and the Mnt surface. The interlayer microscopic structures and mobilities of DDBA-Mnts as a function of DDBA loadings were systematically investigated using classical molecular dynamics simulations. We obtain various interlayer configurations and dynamic information for different number densities of the interlayer DDBA.

Methodology

Organic-Mnt model

The chemical formula of Mnt is $Na_{1.0}(Al_{3.0}Mg_{1.0})Si_8O_{20}(OH)_4$, where Na^+ can be replaced by a monovalent DDBA cation, $Na_{1.0-n}(DDBA)_n(Al_{3.0}Mg_{1.0})Si_8O_{20}(OH)_4$, which was equal to one unit cell (n was the fraction of DDBA in the unit cell). The supercell used for simulation consisted of two clay platelets each containing 24 unit cells: 6 in the x-dimension, 4 in the y-dimension and 2 in the z-dimension. The system contained two interlayer spaces (Fig. 1a). Twenty-four isomorphic substitutions of Mg(II) for Al(III) were imposed in each sheet, which resulted in a layer charge density of −1e/unit cell. Figure 1b shows the molecular structure of DDBA. To probe the interlayer structure of DDBA-Mnt as a function of DDBA loading and to ensure that different interlayer arrangement configurations could be reproduced, we have specified the numbers of DDBA between layers as 6 (0.25 cation-exchange capacity; CEC), 13 (0.54 CEC), 24 (1.00 CEC) and 34 (1.42 CEC), for comparison with the experimental findings of Li *et al.* (2021; denoted as DA-6, DA-13, DA-24, DA-34). Cl^- was used to compensate for the net charge of the system. The initial basal spacing was set

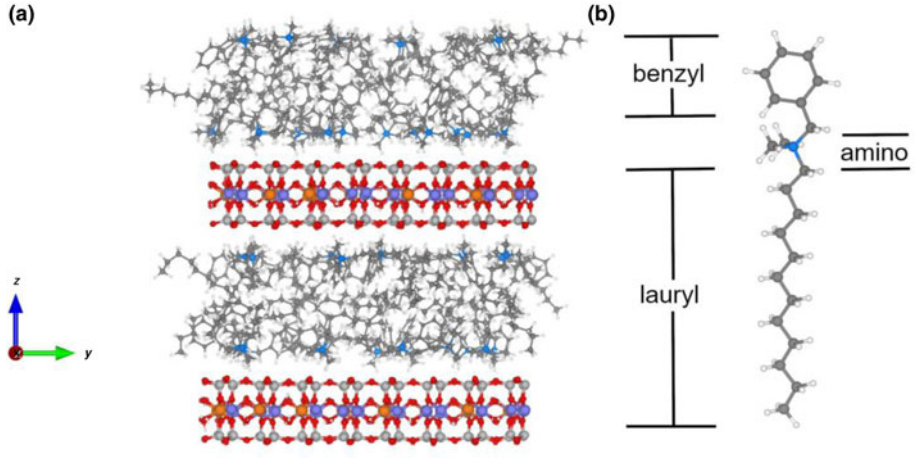

Figure 1. (a) Image of Mnt intercalated with 24 DDBA ions. (b) Structure of the DDBA ion; C = grey, N = blue, H = white, O = red, Si = silver, Mg = orange, Al = ice-blue.

to 50 Å, which was large enough to accommodate the intercalated organic ions. The results presented are the averages of those obtained from each interlayer.

Data analysis

The distribution of interlayer species in space is characterized by the atomic number density distribution along the z-direction (normal to the clay basal plane), which is calculated by averaging the NVT (canonical ensemble with constant particle number, volume and temperature) trajectories, taking the plane where the oxygen atoms in the silicon–oxygen ring at the bottom of the Mnt layer are as the starting plane ($z = 0$).

The formula for the distribution of species number density between layers is as in Equation 1:

$$\rho(z) = \frac{\left\langle N\left(\frac{z-\Delta z}{2}, \frac{z+\Delta z}{2}\right)\right\rangle}{\Delta z \times S} \quad (1)$$

Here, $N\left(\frac{z-\Delta z}{2}, \frac{z+\Delta z}{2}\right)$ is the average number of atoms appearing at the height interval $\left(\frac{z-\Delta z}{2}, \frac{z+\Delta z}{2}\right)$ ($\Delta z = 0.2$ Å in this research) and S is the basal surface area.

The angle between the benzyl group and the clay surface is obtained by the following calculation formula (Equations 2 & 3):

$$\cos(\theta) = \frac{\mathbf{a} \cdot \mathbf{b}}{|\mathbf{a}||\mathbf{b}|} \quad (2)$$

$$\theta = 90^\circ - |90^\circ - \arccos(\theta)| \quad (3)$$

Here, the vectors **a** and **b** are, respectively, the normal vector of the plane where the benzyl ring is located and the normal vector of the plane where the clay layer is located. $|^*|$ is the absolute value.

The radial distribution function (RDF) of species B around species A is as per Equation 4 (Allen & Tildesley, 1987):

$$G_{(AB)}(r) = \frac{1}{4\pi\rho_B r^2}\frac{dn_{AB}}{dr} \quad (4)$$

ρ_B is the average number density of species B, dn_{AB} is the average number density of species B within the range r to $r + dr$ from species A.

The self-diffusion coefficient D of interlayer species can be obtained using the Einstein relationship (Equation 5; Allen & Tildesley, 1987; Chang *et al.*, 1997):

$$\frac{1}{N}\sum_{i=1}^{N}\langle|r_i(t) - r_i(0)|^2\rangle = 2dDt \quad (5)$$

Here, N is the number of atoms and $r_i(t)$ is the centre-of-mass position of the ith atom at time t. d is the diffusion dimension. For example, $d = 3$ represents the total coefficient and $d = 1$ represents the coefficient components in the x-, y- or z-directions, respectively. The left-hand side of Equation 5 is the mean square displacement (MSD) term. The components of MSD in each individual direction are denoted as XX, YY and ZZ. The motion parallel to the x–y plane is obtained by calculating $(XX + YY)/2$.

Computational details

All molecular dynamics simulations were carried out by using the 'Lammps' package (Plimpton, 1995). ClayFF–CVFF was employed to describe the interactions in the systems. The cut-off of short-range interactions was 10.0 Å. The electrostatic interaction was calculated using the Ewald summation method (Frenkel & Smit, 2002) and the number of K-space vectors was determined to reach a precision of $1.0E^{-4}$.

The NPT (ensemble with constant particle numbers, pressure and temperature) simulations were performed at 298 K (temperature) and 1.01325×10^5 Pa (pressure) for 30.0 ns to obtain the basal spacing in equilibrium. After NPT simulations, the NVT simulations at 298 K were carried out for another 15.0 ns for production (structures and dynamics). The time step was set to 0.5 fs in each simulation. Every atom was allowed to move freely.

Results and discussion

Basal spacings

The calculated basal spacings of DDBA-Mnt are given in Table 1. The basal spacing of DDBA-Mnt increased as the loading of DDBA increased. The basal spacing of the DA-6 system was calculated to be 14.1 Å. A small amount of DDBA in the DA-6 system formed a monolayer configuration with a basal spacing similar to that of Na-Mnt, which contained two layers of water in the interlayer (Fu *et al.*, 1990; Sato *et al.*, 1992). The basal spacing of Mnt with a single layer of DDBA between layers obtained by Tahani *et al.* (1999) was ~14.6 Å. This was in a good agreement with the simulation results.

The basal spacings of DA-13, DA-24 and DA-34 were 17.7, 22.5 and 28.2 Å, respectively. The basal spacings of DA-13, DA-24 and DA-34 were 17.7, 22.5 and 28.2 Å, respectively. Tahani *et al.* (1999) obtained a basal spacing of 18 Å for the double layer. Li *et al.* (2021) obtained 17.3, 22.4, 23.1, 23.4 and 29.7 Å basal spacings at various DDBA loadings (all samples above from these works were dried before XRD measurements so that there were almost no interlayer water molecules). For the same interlayer DDBA layered arrangement, the deviations between the calculated values and the experimental values of the basal spacings were all <5%, which means that they were in good agreement.

To illustrate the interlayer structure of DDBA-intercalated Mnt, the simulation focused more on the different configurations of the DDBA arrangement between Mnt layers and the corresponding ranges (plateaus) of basal spacings. The basal spacings obtained by simulation match the basal spacing ranges related to various interlayer configurations obtained in previous experiments, which verifies that the ClayFF–CVFF force field accurately reproduces the microstructure of DDBA-intercalated Mnt. DDBA

Table 1. Simulated basal spacings of DDBA-Mnt.

Amount of interlayer DDBA	Configuration of DDBA arrangement	Basal spacing of simulation (Å)	Basal spacing of experiment (Å)
0.25 CEC	Monolayer	14.1	14.6[a]
0.54 CEC	Bilayer	17.7	17.3[b]
1.00 CEC	Pseudo-trilayer	22.5	22.4[b], 23.1[b], 23.4[b]
1.42 CEC	Pseudo-quadrilayer	28.2	29.7[b]

[a]From Tahani *et al.* (1999).
[b]From Li *et al.* (2021).

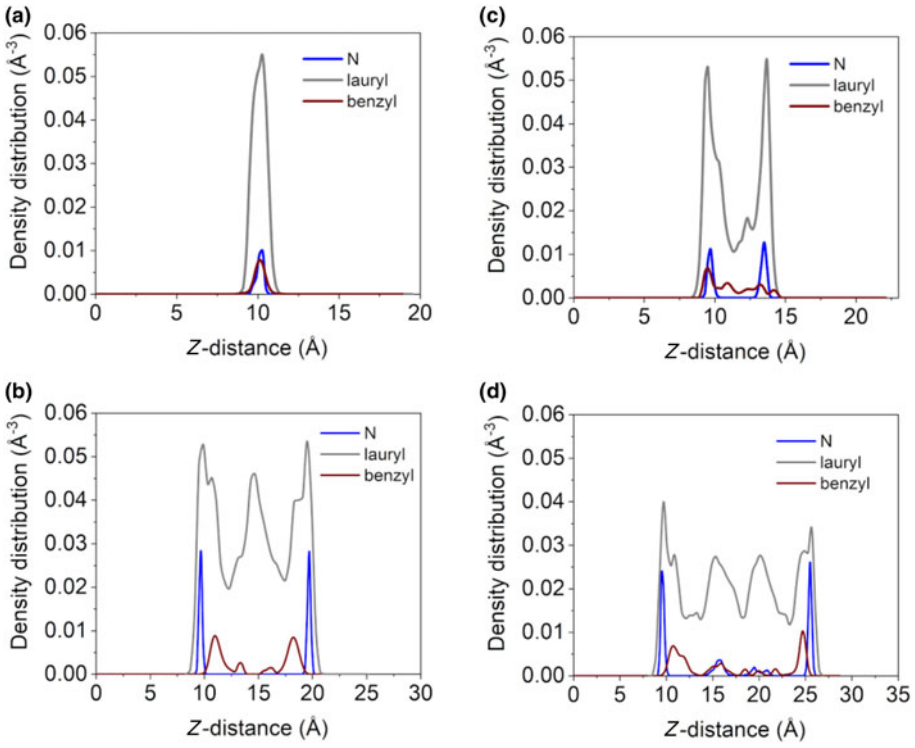

Figure 2. *Z*–density distribution of the N atom, lauryl and benzyl in the different DDBA-intercalated Mnt systems: (a) DA-6 system; (b) DA-13 system; (c) DA-24 system; and (d) DA-34 system.

cations formed layered configurations in the interlayer region, which explains the plateaus observed on the experimental basal spacing curves as a function of DDBA loading.

Interlayer structures

DDBA could form layered configurations in the interlayer region of Mnt. To demonstrate the layering behaviour, we calculated the atomic number density along the *z*-axis (Fig. 2). The ammonium group, lauryl group and benzyl group were represented by N atoms, chain C atoms of the lauryl group and ring C atoms, respectively. In the DA-6 system, all three groups presented single and clear peaks (Fig. 2a), suggesting a monolayer configuration in the interlayer region (Fig. 3a). With the increase of interlayer DDBA loadings, the lauryl group showed two, three and four clear peaks in the DA-13, DA-24, and DA-34 systems, respectively (Fig. 2b–d), corresponding to the bilayer, pseudo-trilayer and pseudo-quadrilayer configurations in the interlayer region (Fig. 3b–d). Based on the experimental measurements on DDBA-Mnt, Tahani *et al.* (1999) proposed configurations of the

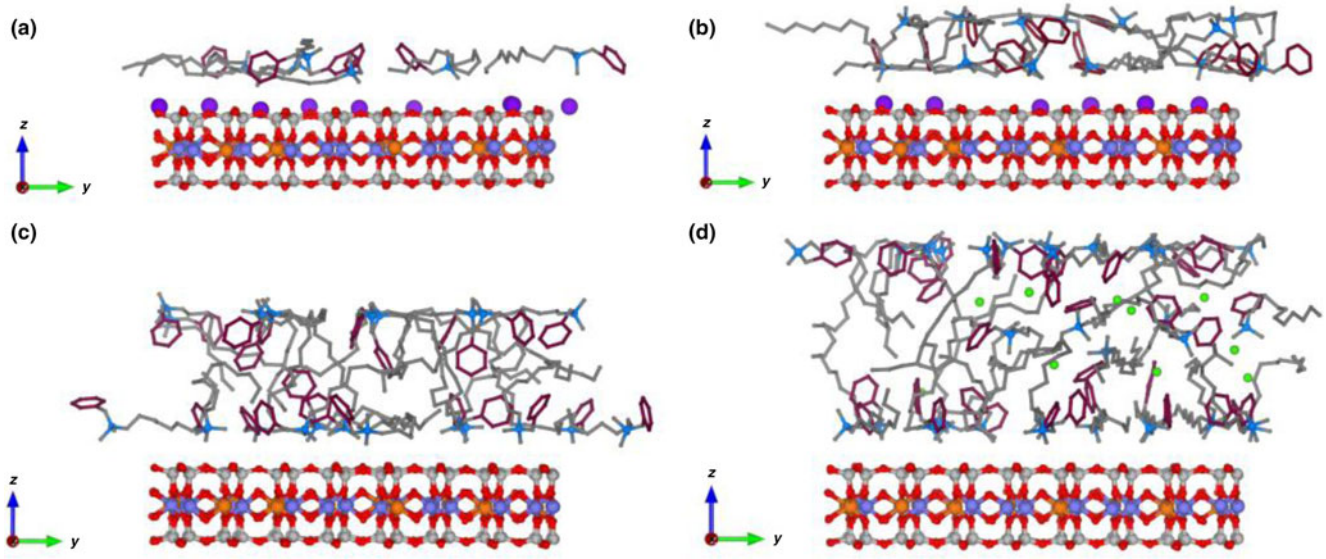

Figure 3. Images of Mnt intercalated with DDBA. All H atoms are removed for clarity. (a) DA-6 system; (b) DA-13 system; (c) DA-24 system; and (d) DA-34 system. C = grey, C (benzyl) = brown, N = blue, O = red, Si = silver, Mg = orange, Al = ice-blue, Na = purple, Cl = green. (Due to the similarity of the interlayer structures in the same system and to show the interlayer structure more clearly, only images of single layers are shown.)

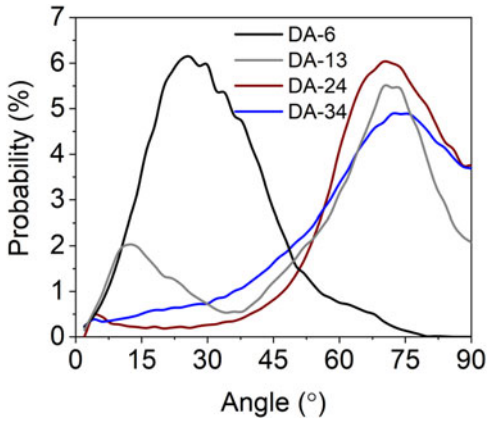

Figure 4. Occurrence probabilities of the angle between the benzyl of DDBA and the clay mineral layer.

DDBA arrangement: DDBA cations changed from lying flat on the surface to perpendicular to the surface with increasing loadings. The structure perpendicular to the surface (pseudo-quadrilayer) could be regarded as a paraffin-type structure. The appearance of the pseudo-quadrilayer (paraffin-type) was attributed to excess unattached DDBA in the middle region rather than vertically and attached to the clay surface (Lagaly *et al.*, 1986).

In the DA-13, DA-24 and DA-34 systems, the lauryl chains presented incompletely separated peaks, suggesting the formation of a non-monolayer structure and the presence of intersecting chains in the middle of the interlayer space. As shown in Fig 3d, the ammonium groups were attached to the upper and lower inner surfaces of the clay mineral, and the alkyl chains were alternately oblique to the (001) surface of the clay minerals, indicating a paraffin-type arrangement (Lagaly *et al.*, 1986). This paraffin-type arrangement was commonly observed in the cases of excessive adsorption of long-chain organic matter into the Mnt interlayer space (Lagaly *et al.*, 2006; He *et al.*, 2010; Huskić *et al.*, 2012; Li *et al.*, 2019). This indicated that the pseudo-quadrilayer arrangement included the paraffin-type configuration of DDBA adsorbed on the upper and lower surfaces and the unattached DDBA configuration in the middle region.

The ammonium group also showed clear peaks in these systems. In the DA-13 and DA-24 systems, two peaks of the N atom of the quaternary ammonium were present (Figs 2b,c & 3b,c), and these peaks were close to the clay basal surfaces, indicating the strong electrostatic interaction between the ammonium and clay surface. In the DA-34 system, the three tiny N peaks in the middle correspond to the N atoms of DDBA in the middle of the interlayer space, which are due to excessive loading in the interlayer space.

Compared to the ammonium group and lauryl group, the peaks of the benzyl group were less well-defined. The curves indicated that the benzyl group was located preferentially on the surface as it was anchored by the ammonium group. Such configurations could be utilized to effectively adsorb aromatic pollutants. Thus, the orientation of the benzyl group relative to the clay surface might play a significant role in the adsorption of aromatic organic compounds on DDBA-intercalated Mnt.

The occurrence probabilities of the angle between the benzyl group and the clay surface are shown in Fig. 4a. As the density of DDBA increased, the average angle between the benzyl group and the clay surface gradually increased. In the DA-6 system, the benzyl groups intersected with the clay surface at a small angle, ranging from 15° to 45° (peaking at 32°; Fig. 4a). With high DDBA number density, the benzyl groups were tilted or even nearly perpendicular to the clay surface, and the angle of inclination ranged from 60° to 90° (peaking at 75°; Fig. 4b).

Interaction mechanisms

The interaction mechanisms of DDBA with clay mineral surfaces can be explored using the RDF for surface oxygen atoms of the

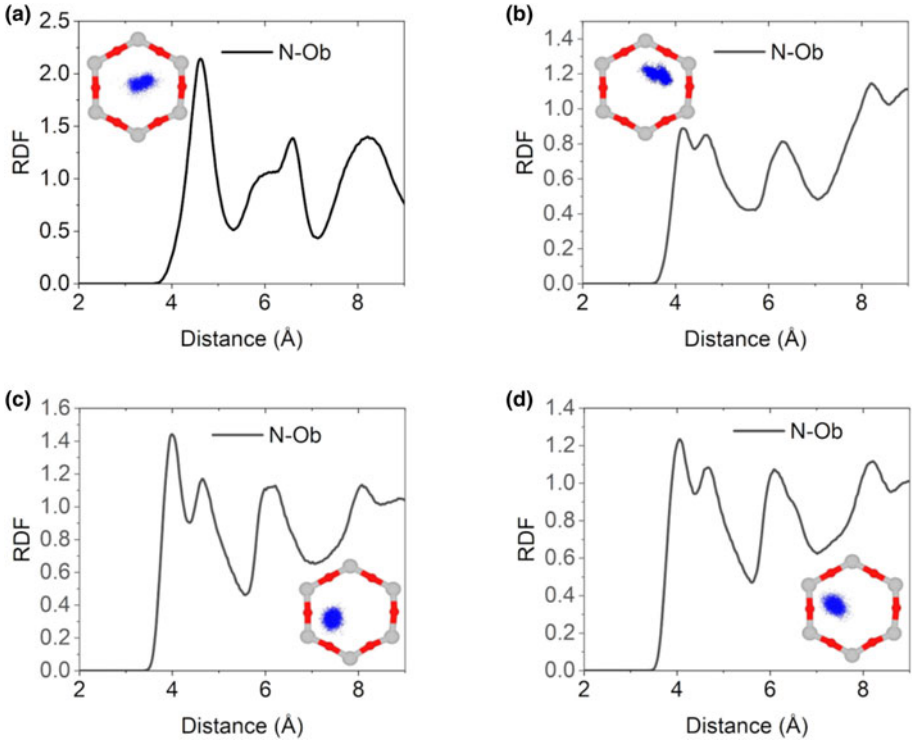

Figure 5. RDFs for surface oxygen atoms of the clay mineral layer (bridging oxygen; Ob) around the N atom of DDBA in the various DDBA-Mnt systems (the blue dots in the images are the overlapped trajectories of the N atoms in the DDBA projected on the *x*–*y* plane). (a) DA-6 system; (b) DA-13 system; (c) DA-24 system; and (d) DA-34 system.

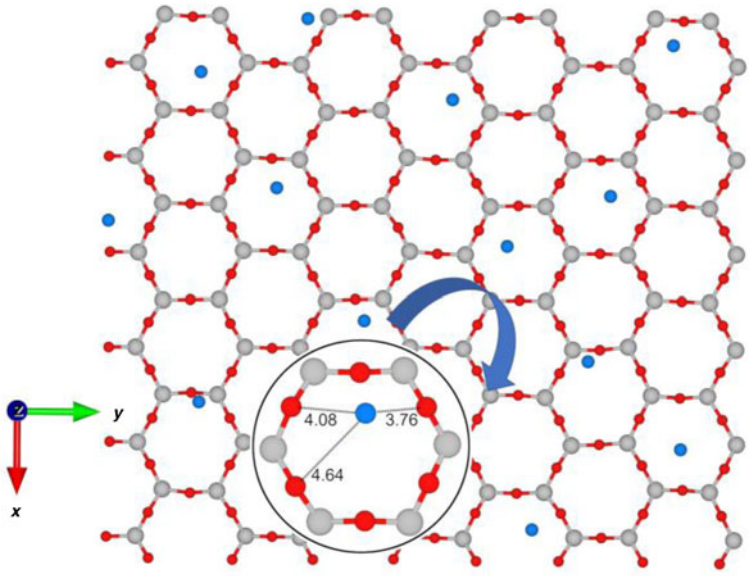

Figure 6. Image of the coordination between the quaternary ammonium N atoms of DDBA and O atoms on the surface of Mnt in the DA-24 system.

clay layer (bridging oxygen; Ob) around the N atoms of DDBA. In the RDF plot (Fig. 5), the first peaks of the RDF curves in the DA-13, DA-24 and DA-34 systems split into two peaks with different heights. This is because the N atoms of DDBA were slightly off-centre from the surface six-member ring. As shown in Fig. 6, the two peaks were at ~3.8–4.0 and ~4.7–4.9 Å, denoting the nearby and far side surface O, respectively. By contrast, the DA-6 system shows a much sharper first peak, indicating that the N atoms of DDBA were located nearly above the centre of the surface six-member ring. These findings were supported by images of the overlapped trajectories of N atoms in DDBA projected onto the x–y plane (blue dots in Fig. 5).

The position of the quaternary ammonium N atom in DDBA deviated from the centre of the six-membered ring on the clay surface. This was due to the two asymmetric groups bonded to the N atom (i.e. the benzyl and lauryl chains were significantly different).

Mobility of interlayer DDBA

Figure 7 shows the self-diffusion coefficients derived from the MSDs (in Fig. S1). In each system, the self-diffusion coefficient of the lauryl chain was the highest and that of the N atom was the lowest. The total self-diffusion coefficient of N atoms in each system was extremely low, ranging from 0.05×10^{-12} to 0.7×10^{-12} m^2 s^{-1}. The total self-diffusion coefficients of the C

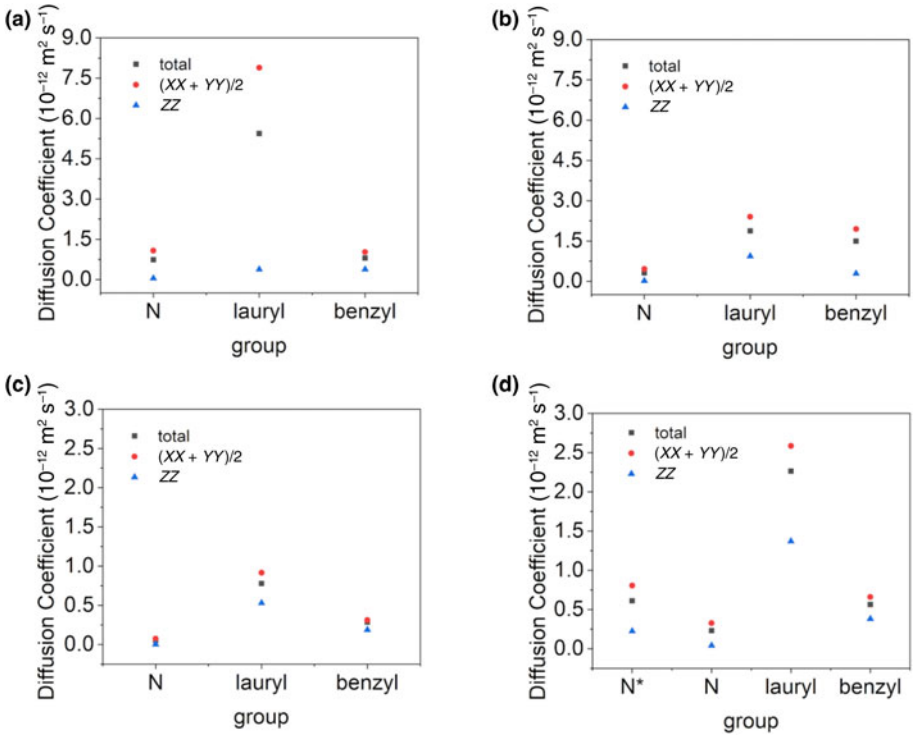

Figure 7. The self-diffusion coefficients of interlayer DDBA in DDBA-Mnt systems (N* = N atoms of DDBA that were not attached to the clay mineral surface). (a) DA-6 system; (b) DA-13 system; (c) DA-24 system; and (d) DA-34 system.

atom in the lauryl chain in DA-6, DA-13, DA-24 and DA-34 were $\sim 5.4 \times 10^{-12}$, 1.9×10^{-12}, 0.9×10^{-12} and 2.3×10^{-12} m^2 s^{-1}, respectively. The total self-diffusion coefficients of the benzyl C were $\sim 0.8 \times 10^{-12}$, 1.5×10^{-12}, 0.3×10^{-12} and 0.6×10^{-12} m^2 s^{-1} in the DA-6, DA-13, DA-24 and DA-34 systems, respectively.

In each system, the $(XX + YY)/2$ component of the self-diffusion coefficient was higher than the ZZ component because of the 2D geometry of the interlayer space. The densities of the organic phases formed by the lauryl chain were 0.22, 0.27, 0.35 and 0.37 g mL^{-1} in interlayer spaces of the DA-6, DA-13, DA-24 and DA-34 systems, respectively (the calculation details can be found in the Supplementary Information). Therefore, in the DA-6 system, the lauryl chain presented the highest $(XX + YY)/2$ component of the self-diffusion coefficient due to it having the lowest density.

Conclusion

The interlayer structures and dynamics of DDBA-Mnt were derived from systematic molecular dynamics simulations. The conclusions are as follows:

(1) DDBA shows layering behaviour in the interlayer region. With increased loadings, the basal spacing of DDBA-Mnt increased and DDBA formed monolayer, bilayer, pseudo-trilayer and pseudo-quadrilayer configurations in the interlayer space sequentially. The basal spacings of DDBA-Mnts matched well with previously reported XRD experimental ranges of basal spacings. Moreover, the pseudo-quadrilayer (paraffin-type) structure was confirmed as a common configuration with overloaded long-chain alkylammonium compounds. The ammonium group and benzyl group preferred to stay above the clay mineral surfaces, whereas the lauryl group, due to its flexible nature, was distributed evenly in the interlayer space.
(2) DDBA ions were anchored to the basal surface through ammonium groups, which were located slightly off-centre from the Si–O six-member ring. The benzyl group and lauryl group were oriented in parallel to the monolayer configuration, whereas in the multilayer configurations they were tilted and pointing towards the interlayer.
(3) The interlayer mobility of DDBA was found to be very low. Specifically, within the DDBA ions, the mobility of the amino group was the lowest, followed by the benzyl group, whereas the mobility of the lauryl group was the highest.

The Mnt surface has obvious confinement effects on DDBA, leading to the generation of a hydrophobic interlayer. The interlayer space of DDBA-intercalated Mnt can enhance the adsorption of other organic molecules due to the strongly hydrophobic alkyl chains and benzyl groups. DDBA, as the main component of disinfectants, is often used to sterilize skin wounds (e.g. benzalkonium chloride, the active ingredient in Band-Aids). Understanding the structure and mobility of DDBA cations in Mnt interlayers is helpful for the design of and research into adsorbing small-molecule drugs on DDBA-modified Mnt.

Supplementary material. The supplementary material for this article can be found at https://doi.org/10.1180/clm.2023.38.

Acknowledgements. We are grateful to the High-Performance Computing Center (HPCC) of Nanjing University for performing the numerical calculations for this paper on its blade cluster system. We thank the help from Professor Xiancai Lu.

Financial support. This study was supported by the project funded by the China Postdoctoral Science Foundation (No. BX20190151) and the National Natural Science Foundation of China (No. 42172050 and 42002036). We acknowledge the financial support from the State Key Laboratory for Mineral Deposits Research at Nanjing University.

Conflicts of interest. The authors declare none.

References

Allen M.P. & Tildesley D.J. (1987) *Computer Simulation of Liquids*. Clarendon Press, Oxford, UK, 385 pp.

Bala P., Samantaraya B.K. & Srivastava S.K. (2000) Synthesis and characterization of Na-montmorillonite-alkylammonium intercalation compounds. *Materials Research Bulletin*, **15**, 1717–1724.

Barber O.W. & Hartmann E.M. (2022) Benzalkonium chloride: a systematic review of its environmental entry through wastewater treatment, potential impact, and mitigation strategies. *Critical Reviews in Environmental Science and Technology*, **52**, 2691–2719.

Barrer R.M. & MacLeod D.M. (1995) Activation of montmorillonite by ion exchange and sorption complexes of tetra-alkyl ammonium montmorillonites. *Transactions of the Faraday Society*, **51**, 1290–1300.

Bhatt J., Somani R.S., Mody H.M. & Bajaj H.C. (2013) Rheological study of organoclays prepared from Indian bentonite: effect of dispersing methods. *Applied Clay Science*, **83–84**, 106–114.

Brigatti M.F., Galan E. & Theng B.K.G. (2006) Structures and mineralogy of clay minerals. Pp. 19–86 in: *Handbook of Clay Science. Development in Clay Science* (F. Bergaya, B.K.G. Theng & G. Lagaly, editors). Elsevier, Amsterdam, The Netherlands.

Chang F.-R.C., Skipper N.T. & Sposito G. (1997) Monte Carlo and molecular dynamics simulations of interfacial structure in lithium-montmorillonite hydrates. *Langmuir*, **13**, 2074–2082.

Chun Y., Sheng G. & Boyd S.A. (2003) Sorptive characteristics of tetraalkylammonium-exchanged smectite clays. *Clays and Clay Minerals*, **51**, 415–420.

Cornell W.D., Cieplak P., Bayly C.I., Gould I.R., Merz K.M., Ferguson D.M. *et al.* (1995) A second generation force field for the simulation of proteins, nucleic acids, and organic molecules. *Journal of the American Chemical Society*, **117**, 5179–5197.

Cygan R.T., Liang J.J. & Kalinichev A.G. (2004) Molecular models of hydroxide, oxyhydroxide, and clay phases and the development of a general force field. *Journal of Physical Chemistry B*, **108**, 1255–1266.

Cygan R.T., Romanov V.N. & Myshakin E.M. (2012) Molecular simulation of carbon dioxide capture by montmorillonite using an accurate and flexible force field. *Journal of Physical Chemistry C*, **116**, 13079–13091.

Cygan R.T., Greathouse J.A. & Kalinichev A.G. (2021) Advances in ClayFF molecular simulation of layered and nanoporous materials and their aqueous interfaces. *Journal of Physical Chemistry C*, **125**, 17573–17589.

Dauber-Osguthorpe P., Roberts V.A., Osguthorpe D.J., Wolff J., Genest M. & Hagler A.T. (1988) Structure and energetics of ligand binding to proteins: *E. coli* dihydrofolate reductase-trimethoprim, a drug–receptor system. *Proteins: Structure, Function and Genetics*, **4**, 31–47.

Fellah M., Hezil N., Guerfi K., Djellabi R., Montagne A., Iost A. *et al.* (2021) Mechanistic pathways of cationic and anionic surfactants sorption by kaolinite in water. *Environmental Science and Pollution Research*, **28**, 7307–7321.

Flores F.M., Loveira E.L., Yarza F., Candal R. & Torres Sánchez R.M. (2017) Benzalkonium chloride surface adsorption and release by two montmorillonites and their modified organomontmorillonites. *Water, Air, & Soil Pollution*, **228**, 42.

Frenkel D. & Smit B. (2002) *Understanding Molecular Simulation*, 2nd edition. Academic Press, New York, NY, USA, 638 pp.

Fu M.H., Zhang Z.Z. & Low P. F. (1990) Changes in the properties of a montmorillonite – water system during the adsorption and desorption of water: hysteresis. *Clays and Clay Minerals*, **38**, 486–492.

Ghavami M., Zhao Q., Javadi S., Jangam J.S.D., Jasinski J.B. & Saraei N. (2017) Change of organobentonite interlayer microstructure induced by sorption of aromatic and petroleum hydrocarbons – a combined study of laboratory characterization and molecular dynamics simulations. *Colloids and Surfaces A: Physicochemical and Engineering Aspects*, **520**, 324–334.

Giese R.F. & Van Oss C.J. (2002) *Colloid and Surface Properties of Clays and Related Minerals*. CRC Press, Boca Raton, FL, USA, 312 pp.

Gieseking J.E. (1939) The mechanism of cation exchange in the montmorillonite–beidellite–nontronite type of clay minerals. *Soil Science*, **47**, 1–14.

Hackett E., Manias E. & Giannelis E.P. (1998) Molecular dynamics simulations of organically modified layered silicates. *Journal of Chemical Physics*, **108**, 7410–7415.

He H.P., Ma Y., Zhu J., Yuan P. & Qing Y. (2010) Organoclays prepared from montmorillonites with different cation exchange capacity and surfactant configuration, *Applied Clay Science*, **48**, 67–72.

Heinz H., Vaia R.A. & Farmer B.L. (2006) Interaction energy and surface reconstruction between sheets of layered silicates. *Journal of Chemical Physics*, **124**, 224713.

Huang Y., Ma X.Y., Liang G.Z. & Yan H.X. (2007) Interactions in organic rectorite composite gel polymer electrolyte. *Clay Minerals*, **42**, 463–470.

Huang Y., Ma X.Y., Liang G.Z. & Yan H.X. (2008) Adsorption of phenol with modified rectorite from aqueous solution. *Chemical Engineering Journal*, **141**, 1–8.

Huang Y., Ma X.Y., Liang G.Z. & Yan H.X. (2009) Structure and properties of polypropylene/organic rectorite nanocomposites. *Clay Minerals*, **44**, 35–50.

Huang Y., Wang X., He X. & Yang Y. (2010) Gel polymer electrolyte based on poly(methyl methacrylate-maleic anhydride)–poly(ethylene glycol) monomethyl ether and organophilic rectorite clay. *Clay Minerals*, **45**, 431–440.

Huskić M., Žagar E. & Žigon M. (2012) The influence of a quaternary ammonium salt and MMT on the *in situ* intercalative polymerization of PMMA. *European Polymer Journal*, **48**, 1555–1560.

Ilari R., Etcheverry M., Waiman V.C. & Zanini G. (2021) A simple cation exchange model to assess the competitive adsorption between the herbicide paraquat and the biocide benzalkonium chloride on montmorillonite. *Colloids and Surfaces A: Physicochemical and Engineering Aspects*, **611**, 125797.

Khan A.H., Macfie S.M. & Ray M.B. (2017) Sorption and leaching of benzalkonium chlorides in agricultural soils. *Journal of Environmental Management*, **196**, 26–35.

Kung K.H.S. & Hayes K.F. (1993) Fourier-transform infrared spectroscopic study of the adsorption of cetyltrimethylammonium bromide and cetylpyridinium chloride on silica. *Langmuir*, **9**, 263–267.

Kwolek T., Hodorowicz M., Stadnicka K. & Czapkiewicz J. (2003) Adsorption isotherms of homologous alkyldimethylbenzylammonium bromides on sodium montmorillonite. *Journal of Colloid and Interface Science*, **264**, 14–19.

Lagaly G. (1986) Interaction of alkylamines with different types of layered compounds. *Solid State Ionics*, **22**, 43–51.

Lagaly G. (1994) Layer charge determination by alkylammonium ions. Pp. 1–46 in: *Layer Charge Characteristics of 2:1 Silicate Clay Minerals* (A.R. Mermut, editor). Clay Minerals Society, Aurora, CO, USA.

Lagaly G. & Weiss A. (1971) Anordnung und Orientierung kationischer Tenside auf Silicatoberflächen. *Kolloid-Z.u.Z.Polymere*, **243**, 48–55.

Lagaly G., Ogawa M. & Dékány I. (2006) Clay mineral organic interactions. Pp. 309–377 in: *Handbook of Clay Science* (F. Bergaya & G. Lagaly, editors). Elsevier, Amsterdam, The Netherlands.

Laird D.A., Scott A.D. & Fenton T.E. (1989) Evaluation of the alkylammonium method of determining layer charge. *Clays and Clay Minerals*, **37**, 41–46.

Lanson B., Mignon P., Velde M., Bauer A., Lanson M., Findling N. & del Valle C.P. (2022) Determination of layer charge density in expandable phyllosilicates with alkylammonium ions: a combined experimental and theoretical assessment of the method. *Applied Clay Science*, **229**, 106665.

Li P., Khan M.A., Xia M., Lei W., Zhu S. & Wang F. (2019) Efficient preparation and molecular dynamic (MD) simulations of Gemini surfactant modified layered montmorillonite to potentially remove emerging organic contaminants from wastewater. *Ceramics International*, **45**, 10782–10791.

Li Y., Shi M.X., Xia M.Z. & Wang F.Y. (2021) The enhanced adsorption of ampicillin and amoxicillin on modified montmorillonite with dodecyl dimethyl benzyl ammonium chloride: experimental study and density functional theory calculation. *Advanced Powder Technology*, **32**, 3465–3475.

Liu X.D., Lu X.C., Wang R.C., Zhou H.Q. & Xu S.J. (2007) Interlayer structure and dynamics of alkylammonium-intercalated smectites with and without water: a molecular dynamics study. *Clays and Clay Minerals*, **55**, 554–564.

Minisini B. & Tsobnang F. (2005) Molecular mechanics studies of specific interactions in organomodified clay nanocomposite. *Composites: Part A*, **36**, 531–537.

Nigam V., Setua D.K, Mathur G.N. & Kar K.K. (2004) Epoxy-montmorillonite clay nanocomposites: synthesis and characterization. *Journal of Applied Polymer Science*, **93**, 2201–2210.

Park Y., Ayoko G.A. & Frost R.L. (2011) Application of organoclays for the adsorption of recalcitrant organic molecules from aqueous media. *Journal of Colloid and Interface Science*, **354**, 292–305.

Pearlman D.A., Case D.A., Caldwell J.W., Ross W.S., Cheatham T.E., Debolt S. *et al.* (1995) Amber, a package of computer-programs for applying molecular mechanics, normal-mode analysis, molecular-dynamics and free-energy calculations to simulate the structural and energetic properties of molecules. *Computer Physics Communications*, **91**, 1–41.

Peng C.L., Zhong Y.H. & Min F.F. (2018) Adsorption of alkylamine cations on montmorillonite (001) surface: a density functional theory study. *Applied Clay Science*, **152**, 249–258.

Plimpton S.J. (1995). Fast parallel algorithms for short-range molecular dynamics. *Journal of Computational Physics*, **117**, 1–19.

Sato T., Watanabe T. & Otsuka R. (1992) Effects of layer charge, charge location, and energy change on expansion properties of dioctahedral smectites. *Clays and Clay Minerals*, **40**, 103–113.

Scholtzová E. (2020) Computational modeling of nanoclays. Pp. 139–166 in: *Micro and Nano Technologies Series, Clay Nanoparticles. Properties and Applications* (G. Cavallaro, R. Fakhrullin & P. Pasbakhsh, editors). Elsevier, Amsterdam, The Netherlands.

Scholtzová E., Madejová J., Jankovič L. & Tunega D. (2016) Structural and spectroscopic characterization of montmorillonite intercalated with *n*-butylammonium cations ($n = 1$–4) – modeling and experimental study. *Clays and Clay Minerals*, **64**, 401–412.

Shah K.J., Pan S.Y., Shukla A.D., Shah D.O. & Chiang P.C. (2018) Mechanism of organic pollutants sorption from aqueous solution by cationic tunable organoclays. *Journal of Colloid and Interface Science*, **529**, 90–99.

Silva I.A., Sousa F.K.A., Menezes R.R., Neves G.A., Santana L.N.L. & Ferreira H.C. (2014) Modification of bentonites with nonionic surfactants for use in organic-based drilling fluids. *Applied Clay Science*, **95**, 371–377.

Sun H. (1998) COMPASS: an *ab initio* force-field optimized for condensed-phase applications overview with details on alkane and benzene compounds. *Journal of Physical Chemistry B*, **102**, 7338–7364.

Sun H., Mumby S.J., Maple J.R. & Hagler A.T. (1994) An *ab Initio* CFF93 all-atom force field for polycarbonates. *Journal of the American Chemical Society*, **116**, 2978–2987.

Tahani A., Karroua M., Van Damme H., Levitz P. & Bergaya F. (1999) Adsorption of a cationic surfactant on Na-montmorillonite: inspection of adsorption layer by X-ray and fluorescence spectroscopies. *Journal of Colloid and Interface Science*, **216**, 242–249.

Teich-McGoldrick S.L., Greathouse J.A., Jové-Colón C.F. & Cygan R.T. (2015) Swelling properties of montmorillonite and beidellite clay minerals from molecular simulation: comparison of temperature, interlayer cation, and charge location effects. *Journal of Physical Chemistry C*, **119**, 20880–20891.

Van de Voorde A., Lorgeoux C., Gromaire M. & Chebbo G. (2012) Analysis of quaternary ammonium compounds in urban stormwater samples. *Environmental Pollution*, **164**, 150–157.

Veiskarami M., Sarvi M.N. & Mokhtari A.R. (2016) Influence of the purity of montmorillonite on its surface modification with an alkyl-ammonium salt. *Applied Clay Science*, **120**, 111–120.

Witthuhn B., Klauth P., Pernyeszi T., Vereecken H. & Klumpp E. (2006) Organoclays for aquifer bioremediation: adsorption of chlorobenzene on organoclays and its degradation by *RHODOCOCCUS B*528. *Water, Air & Soil Pollution: Focus*, **6**, 317–329.

Yang S., Liang G., Gu A. & Mao H. (2012) Facile synthesis and catalytic performance of Fe-containing silica-pillared clay derivatives with ordered

interlayer mesoporous structure. *Industrial & Engineering Chemistry Research*, **51**, 15593–15600.

Yang S., Liang G., Gu A. & Mao H. (2013) Synthesis of mesoporous iron-incorporated silica-pillared clay and catalytic performance for phenol hydroxylation. *Applied Surface Science*, **285B**, 721–726.

Yariv S. & Cross H. (2002) *Organo-Clay Complexes and Interactions*. CRC Press, Boca Raton, FL, USA, 680 pp.

Yue X., Zhang R., Li H., Su M., Jin X. & Qin D. (2019) Loading and sustained release of benzyl ammonium chloride (BAC) in nano-clays. *Materials*, **12**, 3780.

Zanini G.P., Ovesenr R.G., Hansen H.C.B. & Strobel B.W. (2013) Adsorption of the disinfectant benzalkonium chloride on montmorillonite. Synergistic effect in mixture of molecules with different chain lengths. *Journal of Environmental Management*, **128**, 100–105.

Zeng J., Li Y., Jin G., Su J.Q. & Yao H. (2022) Short-term benzalkonium chloride (C12) exposure induced the occurrence of wide-spectrum antibiotic resistance in agricultural soils. *Environmental Science & Technology*, **56**, 15054–15063.

Zhou Q., Shen W., Zhu J., Zhu R., He H., Zhou J. & Yuan P. (2014) Structure and dynamic properties of water saturated CTMA-montmorillonite: molecular dynamics simulations. *Applied Clay Science*, **97–98**, 62–76.

Zhu J.X., Zhu L.Z., Zhu R.L. & Chen B.L. (2008) Microstructure of organo-bentonites in water and the effect of steric hindrance on the uptake of organic compounds. *Clays and Clay Minerals*, **56**, 144–154.